Article

Control of Structural and Magnetic Properties of Polycrystalline Co$_2$FeGe Films via Deposition and Annealing Temperatures

Andrii Vovk [1],*[iD], Sergey A. Bunyaev [1][iD], Pavel Štrichovanec [2][iD], Nikolay R. Vovk [1], Bogdan Postolnyi [1,3][iD], Arlete Apolinario [1], José Ángel Pardo [2,4][iD], Pedro Antonio Algarabel [5,6][iD], Gleb N. Kakazei [1] and João Pedro Araujo [1][iD]

[1] Departamento de Física e Astronomia, Institute of Physics for Advanced Materials, Nanotechnology and Photonics (IFIMUP), Universidade do Porto, 4169-007 Porto, Portugal; sergiy.bunyayev@gmail.com (S.A.B.); nikolayvovk94@gmail.com (N.R.V.); b.postolnyi@gmail.com (B.P.); arlete.apolinario@fc.up.pt (A.A.); gleb.kakazei@fc.up.pt (G.N.K.); jearaujo@fc.up.pt (J.P.A.)

[2] Instituto de Nanociencia y Materiales de Aragón, Campus Río Ebro, Universidad de Zaragoza—CSIC, 50018 Zaragoza, Spain; stricho@unizar.es (P.Š.); jpardo@unizar.es (J.Á.P.)

[3] Department of Nanoelectronics and Surface Modification, Sumy State University, 40007 Sumy, Ukraine

[4] Departamento de Ciencia y Tecnología de Materiales y Fluidos, Universidad de Zaragoza, 50018 Zaragoza, Spain

[5] Instituto de Nanociencia y Materiales de Aragón, Campus San Francisco, Universidad de Zaragoza—CSIC, 50009 Zaragoza, Spain; algarabe@unizar.es

[6] Departamento de Física de la Materia Condensada, Universidad de Zaragoza, 50009 Zaragoza, Spain

* Correspondence: ayvovk@fc.up.pt

Abstract: Thin polycrystalline Co$_2$FeGe films with composition close to stoichiometry have been fabricated using magnetron co-sputtering technique. Effects of substrate temperature (T_S) and post-deposition annealing (T_a) on structure, static and dynamic magnetic properties were systematically studied. It is shown that elevated T_S (T_a) promote formation of ordered L2$_1$ crystal structure. Variation of T_S (T_a) allow modification of magnetic properties in a broad range. Saturation magnetization ~920 emu/cm^3 and low magnetization damping parameter α ~ 0.004 were achieved for T_S = 573 K. This in combination with soft ferromagnetic properties (coercivity below 6 Oe) makes the films attractive candidates for spin-transfer torque and magnonic devices.

Keywords: thin films; Heusler alloys; magnetostatic properties; Ferromagnetic resonance

1. Introduction

Full-Heusler alloys (FHA) are ternary intermetallic compounds of composition X$_2$YZ, where X and Y are transition metals and Z is a main-group *sp*—element. Recently they attracted a lot of attention due to unique physical properties suitable for advanced applications (See e.g., [1] and references therein). Some FHAs demonstrate half-metallic ferromagnetic (HMF) properties, that are crucial for spintronics. The term HMF [2] is used to describe a material with strong asymmetry in spin-split band structure. This means that the majority spin band has metallic characteristics (i.e., Fermi level (ε_F) is located within the band with finite density of states (DOS)) but for the minority one, ε_F is situated in a band gap (DOS = 0). This leads to 100% spin polarization of conduction electrons. Half metallicity can be used to enhance key properties of magnetic field sensors based on Giant or Tunneling magnetoresistance effect (GMR/TMR), magnetic random-access memory (MRAM) and spin-transfer torque (STT) devices [3]. Several Co$_2$-based FHA were found to be HMF materials and studied intensively [2,4–8]. Another attractive HMF feature (particularly for magnonic applications [9]) is low values of Gilbert damping parameter (α) [10]. Previously very low α were reported for epitaxial Co$_2$FeAl (α ~ 0.001) [11], Co$_2$MnSi (α ~ 0.0004–0.0025) [12,13] and Co$_2$FeGe (α ~ 0.0025) [5] FHA films. It was shown [14] that α is proportional to the product $\xi^2 D(\varepsilon_F)$, where ξ, is the spin-orbit coupling parameter and

$D(\varepsilon_F)$ is the density of states at Fermi level. While ξ is already low for FHA due to small orbital moments [15], vanishing values of $D(\varepsilon_F)$ in one of the spins channels of HMF reduce α even further. According to the model proposed in [16], one should increase spin polarization and reduce α, saturation magnetization (M_S) and exchange stiffness constant (A) of a ferromagnetic material to achieve a decrease in the critical current (J_c) and minimize the power consumption required for the STT switching. Thus, FHA with high spin polarization and moderate values of M_S and A comparing to ferromagnetic metals like Fe and Co are attractive candidates for STT applications. On the other hand, a large value of α is needed to improve thermal stability in current-perpendicular-to-plane giant magnetoresistance (GMR) read sensors [17] Physical properties of FHA can be effectively tuned in a wide range by changing atomic ordering, microstructure and composition [1,2,4,17–21]. Thus, FHA films are considered as attractive candidates for different multifunctional applications. It was shown in [5,17,19,22,23] that substrate temperature (T_S) and post-deposition annealing (T_a) are powerful tools to control the properties of FHA films. However, so far there is no universal law for thermal treatment conditions. They should be chosen individually depending on composition on the film and preparation strategy.

In this work Co_2FeGe polycrystalline films were fabricated using magnetron co-sputtering at different conditions. Here we report on the control of the structure, static and dynamic magnetic properties via deposition temperature and post-deposition annealing. We found that damping can be tuned in a broad range by adjusting deposition temperature. The values of parameters derived from the experiment were analyzed and compared to those known from the literature.

2. Materials and Methods

Heusler alloy films of composition Co_2FeGe and thickness ~60 nm were grown onto 25×25 mm^2 Corning Glass substrates using Orion-5 deposition system (AJA International Co., Scituate, MA, USA). The system was operated under full computer control allowing programing the deposition sequences and reproduction of the technological conditions with high accuracy. Co-sputtering from two independent sources technique was used for sample preparation. Previously it was shown that this technique is very effective for preparation of different nanostructures [24,25] and Co_2FeGe thin films of various composition [6,20,21]. Deposition was performed from two independent direct current 2″ magnetron sputter sources loaded with high purity (better than 99.99 at. %) Co_2Fe alloy and Ge targets (Testbourne Ltd., Basingstoke, UK). Base pressure was below 2×10^{-7} Torr and the depositions were carried out at 3 mTorr of Ar. The deposition rates were determined from thickness measurements of the reference films. The values of 7.7 nm/min for Co_2Fe and 5.1 nm/min for Ge were selected to ensure stoichiometric composition of the resulting alloy. During film preparation, the rates were kept constant via the control of the deposition current. The substrates were mounted on a rotating sample holder (25 RPM) that was positioned at 120 mm distance from the deposition sources to provide uniformity of the films thickness and composition. Films were deposited at room temperature (RT), and elevated temperatures T_S = 573 K and T_S = 773 K. After deposition the samples were kept 4 h in the chamber in the 3 mTorr Ar atmosphere for cooling. To study the effect of annealing the films were deposited at T_S = RT and annealed in-situ in 3 mTorr Ar flow at T_a = 573 K and T_a = 773 K for 1 h. The cooling sequence was the same as for the films deposited at the elevated T_S.

The composition of the films was checked by Energy Dispersive X-Ray analysis using FEI Quanta 400FEG Field Emission SEM/EDAX-PEGASUS X4M (FEI Co., Hillsboro, OR, USA). X-ray investigations were carried out using Rigaku SmartLab X-ray diffractometer (Rigaku Co., Tokyo, Japan) equipped with a primary Ge crystal monochromator (Cu-Kα radiation). The crystal structure of the films was investigated using grazing incidence X-ray diffraction (GIXRD) in parallel beam geometry with 0.6° incidence angle (right above the maximum critical angle among all the samples, 0.37°). X-ray reflectivity (XRR) measurements were also performed to evaluate thickness, surface oxidation and roughness

of the films. To extract abovementioned parameters the experimental XRR profiles were fitted using LEPTOS software version 2.02 (Bruker AXS GmbH, Karlsruhe, Germany).

Static magnetic characterization of the films was performed using Quantum Design MPMS superconducting quantum interference device magnetometer (Quantum Design Inc., San Diego, CA, USA). Magnetic hysteresis loops were measured at RT and in magnetic field *H* up to 500 Oe applied in the film plane. All spurious instrumental effects and those associated with paramagnetic substrate contribution [26,27] were carefully accounted for and subtracted from the initial magnetization curves.

Ferromagnetic resonance (FMR) measurements were carried out at room temperature using a coplanar waveguide (CPW) connected to a vector network analyzer (VNA) Anritsu 37247D (Anritsu Co. Inc., Atsugi, Japan). A dc magnetic field was applied in film plane perpendicularly to the direction of the magnetic component of the microwave field. The samples were placed film down on the CPW, and the complex S_{21} parameter was measured as a function of the external magnetic field over a frequency range up to 20 GHz. The FMR frequency *f* and resonance linewidth ΔH were extracted from the raw data as described in [28,29].

3. Results and Discussion

3.1. Structural Properties

The composition of the films under investigation (in atomic percent) checked by EDAX varies from $Co_{48}Fe_{23}Ge_{29}$ to $Co_{48}Fe_{21}Ge_{31}$. This slightly differs from targeted stoichiometry $Co_{50}Fe_{25}Ge_{25}$.

Figure 1 shows XRR of the films deposited at different T_S (a) and deposited at RT and annealed at T_a (b).
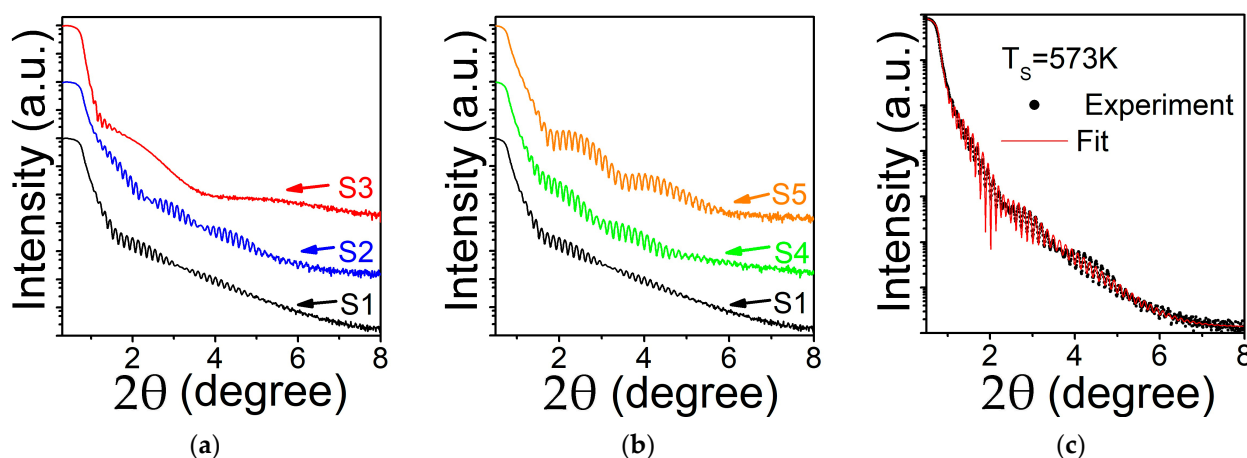
Figure 1. X-ray reflectivity for Co_2FeGe films: (**a**) deposited at T_S = RT (S1), T_S = 573 K (S2), T_S = 773 K (S3); (**b**) deposited at RT and annealed for 1 h at T_a = 573 K (S4), T_a = 773 K (S5); (**c**) fit of the experimental XRR spectrum for the film deposited at T_S = 573 K. Fitting parameters are summarized in Table 1.

Table 1. Structural parameters obtained from XRR and GIXRD in all the samples as a function of the temperature used for deposition (T_S) and annealing (T_a). The film thickness (t), surface roughness (Δt) and density (ρ) were determined from the fits to the experimental XRR patterns with a chi-square value below 3×10^{-2}. The lattice parameter (a) and crystallite size (d) were calculated from GIXRD within ± 0.002 Å and ± 0.5 nm accuracy, respectively.

T_S, K	T_a, K	From XRR			From GIXRD	
		t, nm	Δt, nm	ρ, gr/cm³	a, Å	d, nm
RT	—	57	0.63	8.3	5.732	10
573	—	61	0.47	8.64	5.734	14
773	—	61	2.1	8.66	5.715	15
RT	573	59	0.63	8.31	5.732	11
RT	773	57	0.63	8.69	5.713	13

Films deposited at T_S = RT and 573 K exhibit a periodic pattern in a wide diffraction angle, suggesting a flat layer structure, while the one at T_S = 773 K shows a fast drop and decay of Kiessig oscillations, indicating a rough surface. In addition, there is a visible two period oscillations around $2\theta \approx 3–3.5°$ (T_S = RT) and $2\theta \approx 2.25–2.5°$ and $2\theta \approx 3.5–3.75°$ (T_S = 573 K), which can be interpreted as due to the formation of a thin oxide surface layer. The XRR data for annealed films retain periodic pattern for all T_a but still show two period oscillations. Fit of the experimental data (Figure 1c) allows estimation of thickness, roughness and density. Film and native oxide densities were set as free parameters since the exact chemical composition of the oxide is not known, and the density of the film can be different from the bulk. Bulk densities for Co_3O_4 oxide (6.11 g/cm³) and Co_2FeGe alloy (8.66 g/cm³) were chosen as initial values. The best fitting parameters are presented in Table 1. For all the films the estimated thickness of Co_2FeGe is within 58 nm $\pm$ 3 nm range that corresponds well to targeted 60 nm value. The thickness of native oxide layer was evaluated between 2 and 5 nm with the density ~6.5 g/cm³ for all the samples. The estimated densities of the films deposited at elevated T_S are close to bulk values. However, films deposited at T_S = RT and those annealed afterwards at T_a = 573 K show lower density (as reflected by a slightly smaller critical angle). The former case can be explained as due to smaller diffusion rates of adatoms during deposition, while the latter because relatively low T_a does not provide conditions for efficient re-crystallization. Surface roughness for the films deposited at T_S = RT and for annealed at different T_a was determined to be ~0.63 nm independently of the annealing temperature used in this study. The lowest surface roughness (0.47 nm) was found for the film deposited at T_S = 573 K while for T_S = 773 K it is much higher (~2 nm). Low surface roughness is a key factor for preparation of the electrodes for TMR tunnel junctions [30]. From this aspect the films deposited at T_S = 573 K are the best candidates.

Ordered FHA, X_2YZ (in our case X = Co, Y = Fe, Z = Ge) crystalize in the cubic $L2_1$ structure (space group no. 225, $Fm\bar{3}m$) [31]. However, different variants of disorder are observed when X, Y and/or Z atoms are intermixed. Usually for FHA thin films the following cases of disorder are considered [2]: $B2$-Y and Z atoms are randomly intermixed (space group no. 221, $Pm\bar{3}m$); $A2$-complete disorder with random intermixing (group no. 229, $Im\bar{3}m$). The most noticeable differences in the X-ray patterns for these atomically disordered phases is the absence of some superstructure reflections of the $L2_1$ type structure. Reflexes (111) and (311) are missing for both $B2$ and $A2$ disorders. Additionally, (200), (222) and (420) reflexes are absent for $A2$ disorder. In Figure 2 GIXRD patterns are shown for the films deposited at different T_S (a) and deposited at RT and annealed at T_a (b). It is clearly seen that all the films exhibit fine polycrystalline structure. For the one deposited at T_S = RT only peaks (220) and (400) are observed. This is characteristic of disordered nanocrystalline film of $A2$ structural type. With increasing T_S the width of the reflections decreases and their intensity increases. In addition, superstructure line (111) characteristic for $L2_1$ ordering appears (See close-up in Figure 2c). Similar variations are found for T_a.

However, annealing seems to be less efficient for atomic ordering comparing to deposition at elevated temperature as the superlattice reflection (111) appeared only at T_a = 773 K but is absent for T_a = 573 K (See close-up in Figure 2d). It is worth mentioning that for Co_2FeGe the intensities of $L2_1$ and *B2* superlattice reflections are low due to nearly equal scattering factors of Co, Fe and Ge [32]. From the International Centre for Diffraction Data (ICDD) database one can find [33] for stoichiometric bulk Co_2FeGe alloy I_{111}/I_{220} ~ 0.012, I_{200}/I_{220} ~ 0.0007 and I_{311}/I_{220} ~ 0.0006. In our case for the samples deposited at T_S = 573 K and 773 K experimental value I_{111}/I_{220} is in the range 0.017–0.019 that is somewhat higher comparing to theoretically calculated values. This can be due to slight Ge enrichment of our films. Reflections (200), (311) and (222) were not observed in any sample. Absence of (200) reflection is a characteristic of *B23a* structure (space group no. 227, $Fd\bar{3}m$) which represents a mix of two face centered cubic sublattices. In this structure, the first sublattice is formed with *X* atoms intermixed with *Y* atoms and the second—with *X* atoms intermixed with *Z* atoms. However, this type of atomic order is very uncommon to be experimentally realized [34]. On the other hand, significant variations in the intensities of the (200) and (311) reflections could be achieved in the case of so-called DO_3 or *X*-type disorders [35]. *X*-type structure (space group no. 216, $F\bar{4}3m$) is formed if the atomic number of the *Y* atom is higher than that of the *X* atom, which is not our case. For DO_3 space group $Fm\bar{3}m$ is conserved but *X* and *Y* or *X* and *Z* atoms are mixed on their crystallographic positions. One can suggest formation of disordered *A2* phase for the film deposited at RT. For elevated T_S and T_a a mixture of $L2_1$ and DO_3 phases is formed with reduced intensities of weaker reflections (200) and (311) (which fall below the detection limit of our instrument).
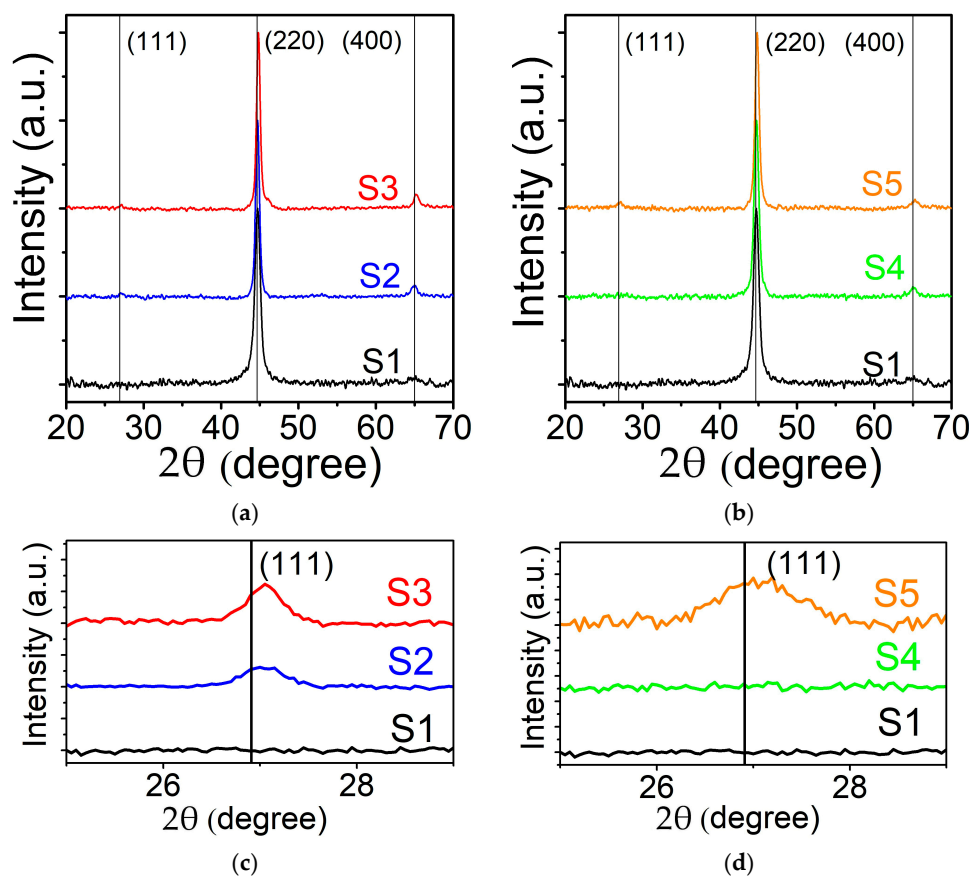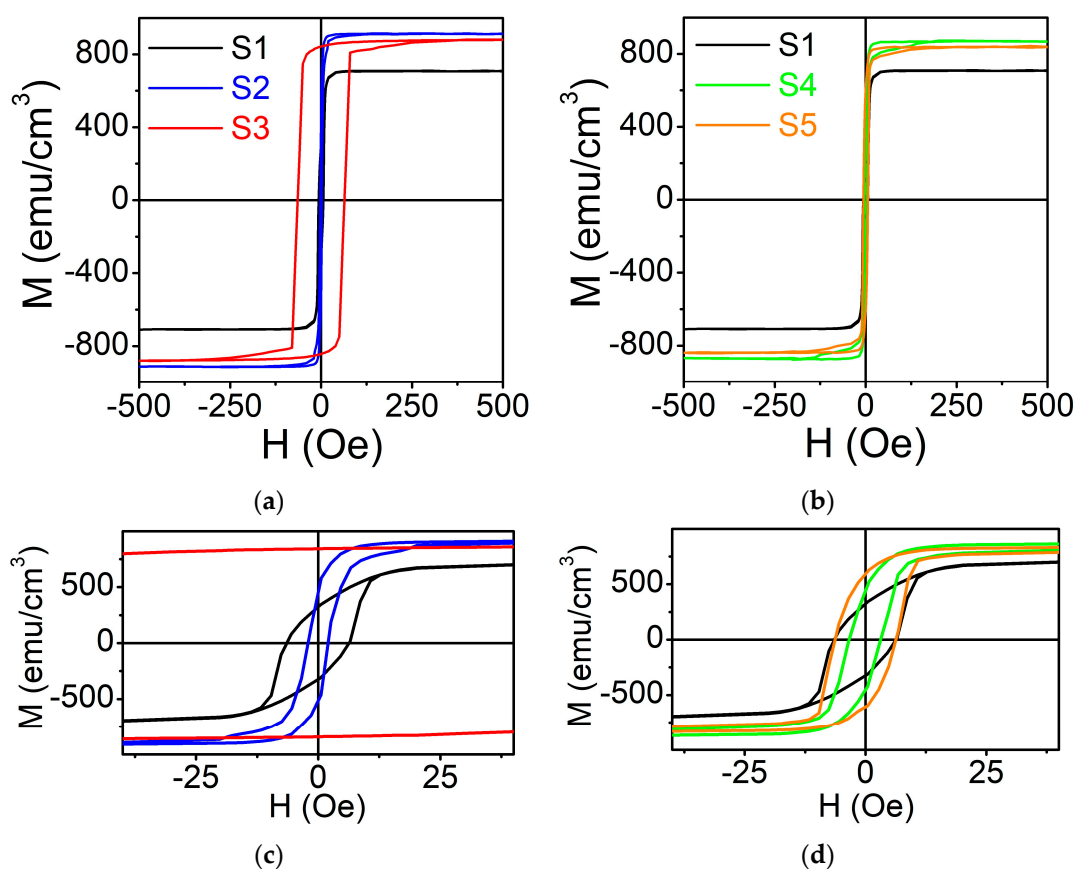

Figure 2. GIXRD patterns for Co_2FeGe films: (**a**) deposited at T_S = RT (S1), T_S = 573 K (S2), T_S = 773 K (S3); (**b**) deposited at RT and annealed for 1 h at T_a = 573 K (S4), T_a = 773 K (S5). Close-ups for (111) reflection area for films: (**c**) deposited at different T_S; (**d**) for films deposited at RT and annealed at different T_a for 1 h.

The evolution of lattice parameters and estimation of crystallite size determined by Scherrer's formula [36] are presented in Table 1. Crystallite size shows expected behavior, i.e., it increases with increasing T_S and T_a. The lattice parameters for the films deposited at T_S = RT and 573 K (a = 5.732 Å and a = 5.734 Å, respectively) correspond fairly well to the bulk stoichiometric alloy values (a = 5.738 Å) reported earlier [37,38] while for T_S = 773 K it is lower (a = 5.715 Å). The same tendency was found for annealed films. One can suggest that this decrease of the lattice parameter for $T_S(T_a)$ = 773 K is a consequence of a compressive stress induced by differences in thermal expansion coefficients for film and Corning Glass substrate. Thus, varying T_S and/or T_a one can control formation of ordered Co_2FeGe $L2_1$ phase, crystallite sizes and surface roughness to produce films with desired properties. In our case T_S = 573 K was found to be optimal to achieve the lowest surface roughness.

3.2. Magnetostatic Properties

In-plane magnetic hysteresis loops measured at RT are shown in Figure 3. Determined values of saturation magnetization (M_S) and coercive field (H_C) are summarized in Table 2. Since exact volume and magnetic properties of the native oxide is not known, the values of M_S were calculated using nominal thickness of 60 nm for all films. All the samples demonstrate ferromagnetic behavior. The film deposited at T_S = RT has the smallest M_S. The value of M_S first increases noticeably with T_S and afterwards slightly drops for T_S = 773 K. All the films under study, except the one deposited at T_S = 773 K (for which the enhanced H_C = 65 Oe was observed), are magnetically soft. The values of H_C were found to be below 6 Oe with minimum of 2 Oe for the film deposited at T_S = 573 K (See close-ups for −30 Oe < H < 30 Oe region in Figure 3c,d).

Figure 3. Magnetic hysteresis loops (M vs. H) for Co_2FeGe films: (**a**) deposited at T_S = RT (S1), T_S = 573 K (S2), T_S = 773 K (S3); (**b**) deposited at RT and annealed for 1 h at T_a = 573 K (S4), T_a = 773 K (S5). Close-ups for −30 Oe < H < 30 Oe region for films: (**c**) deposited at different T_S; (**d**) for films deposited at RT and annealed at different T_a for 1 h.

Table 2. Deposition temperature (T_S), temperature of annealing (T_a), saturation magnetization (M_S) and coercive field (H_C) determined from SQUID measurements, effective magnetization (M_{eff}), exchange stiffness (A) and damping parameter (α) determined from FMR measurements. Error margins for M_S were estimated from uncertainty of the sample size determination. Error margins for FMR measurements were derived from fitting procedure.

T_S, K	T_a, K	From SQUID		From FMR		
		M_S, Emu/cm^3	H_C, Oe	M_{eff}, Emu/cm^3	A, pJ/m	α
RT	—	710 ± 35	6 ± 1	738 ± 10	6.8 ± 0.2	$0.007 \pm 1.5 \times 10^{-4}$
573	—	920 ± 50	2 ± 0.5	895 ± 10	9.2 ± 0.3	$0.004 \pm 1.1 \times 10^{-4}$
773	—	880 ± 45	65 ± 1	930 ± 180	9.3 ± 1.2	$0.06 \pm 6 \times 10^{-3}$
RT	573	870 ± 45	3 ± 0.5	906 ± 10	9.8 ± 0.3	$0.005 \pm 1.7 \times 10^{-4}$
RT	773	840 ± 45	6 ± 1	882 ± 40	9.4 ± 0.3	$0.009 \pm 6 \times 10^{-4}$

The variation of the magnetic properties correlates with microstructural changes. The reduced value of M_S for T_S = RT can be due to fine polycrystalline structure with *A2* type atomic disorder. The increase in M_S with the simultaneous decrease of H_C for T_S = 573 K can be attributed to the growth of the film with lower surface roughness and atomically ordered $L2_1$ structure with larger crystallites. For T_S = 773 K the film was found to be subjected to a compressive stress (pinpointed by the reduced out-of-plane lattice parameter was observed by GIXRD) and with enhanced surface roughness. A combination of these factors could be a reason for the increase of H_C. Similar changes in M_S and H_C with T_a were observed for annealed films. However, the annealing leads to smaller variation of magnetic parameters. Most probably this is because re-crystallization and formation of atomically ordered structure caused by annealing is less effective comparing to deposition at the corresponding T_S.

The highest value of saturation magnetization M_S = 920 emu/cm^3 was observed for the film deposited at T_S = 573 K. This is in good agreement with the results previously reported for Co$_2$FeGe films in [39] while is slightly lower comparing to those from [6,22]. However, in the latter case the films were Co$_2$Fe enriched. According to Slater-Pauling rule, one should expect the saturation magnetization of 6 μ_B/f.u. (μ_B is Bohr magneton and f.u. is formula unit) for Co$_2$FeGe FHA [2]. Considering four atoms per unit cell, experimental values of lattice parameter and applying M_S = 920 emu/cm^3 one obtains M_S~4.7 μ_B/f.u. This value is lower than theoretically predicted and experimentally observed for bulk alloys (5.54 μ_B/u.c.) [37] and foils (5.74 μ_B/u.c.) [40] as well as obtained for Co$_2$Fe enriched films [6]. However, our result is very similar to 4.8 μ_B/u.c. reported for the films prepared by thermally activated intermixed reaction [41]. Reduced magnetization values per f.u. might be caused by the deviation of chemical composition from stoichiometric (i.e., slight Ge enrichment), residual atomic disorder and/or reduction of the magnetic moments on the grain boundaries of the crystallites [7,40–42]. It is to be pointed out that T_S/T_a = 573 K seems to be optimal to produce Co$_2$FeGe thin films with improved magnetic properties. This result is in a good agreement with previously published in [19,23].

3.3. Magnetodynamic Properties

VNA-FMR measurements were carried out in frequency domain at different applied fields H_{ext}. For each field value, real and imaginary parts of effective permeability parameter $U(f)$ was calculated from the measured complex S21 spectra as described in [28]:

$$U(f) = \pm \frac{i \ln\left[S_{21-H}(f)/S_{21-ref}(f)\right]}{\ln\left[S_{21-ref}(f)\right]}, \tag{1}$$

where $S_{21-H}(f)$ denotes the set of S$_{21}$ parameters at the FMR field of interest, and $S_{21-ref}(f)$ is the set of S$_{21}$ parameters at the reference field. The detailed description of the method for a single resonance line analysis, the mathematical expression of the fitting function $U_{fit}(f)$ and field to frequency linewidth conversion are given in [28]. This fitting procedure

provides for each peak the set of the following parameters: FMR frequency f, line width at half maximum Δf and phase shift adjustment φ.

The real part of the typical $U(f)$ spectra for different H_{ext} is presented in Figure 4a.

(a)   (b)
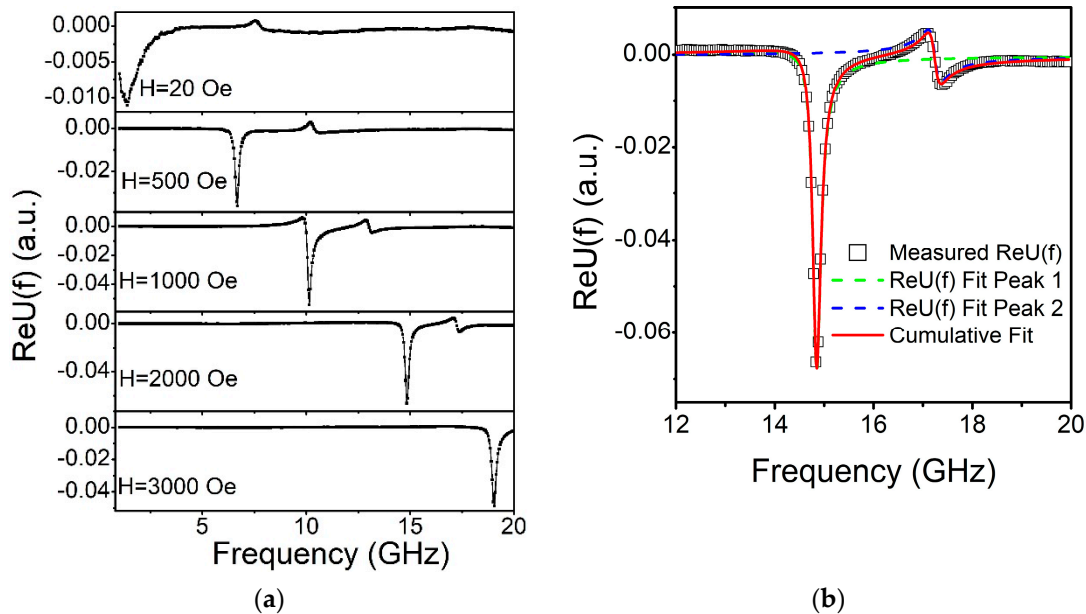
Figure 4. Real part of the *U(f)* function calculated from measured complex S21 spectrum for the film deposited at TS = 573 K at different applied fields (**a**); Example of fitting of permeability Re*U(f)* for the same sample at a static applied field Hext = 2000 Oe (**b**). The open circles represent the Re*U(f)* values extracted from the experimental S21 parameters. The two dashed lines show the best individual fitting functions Re*Ufit(f)* for each peak while the solid curve shows cumulative fit for the whole spectrum.

For all the samples the spectra contain two resonances with visible phase shift between them. Therefore, the sum of two independent fitting functions $U_{fit}(f)$ was used to analyze the data. This approach allows one to evaluate accurately f and Δf even for the case of the vicinity of two peaks with different phases and amplitudes (see an example of the fitting in Figure 4b).

These two resonance peaks were identified as uniform FMR precession (the more intense peak) and first Perpendicular Standing Spin Wave (PSSW) modes. Analysis of the frequency dependence of the main peak on applied magnetic field allows estimation of the effective magnetization M_{eff} of the sample using Kittel's formula [43]:

$$f_{FMR} = \frac{\gamma}{2\pi}\sqrt{\left(H_{ext} + H_{ani}\right)\left(H_{ext} + H_{ani} + 4\pi M_{eff}\right)}$$ (2)

where f_{FMR} is the FMR resonance frequency, γ is the gyromagnetic ratio, H_{ext} and H_{ani} are the applied magnetic field and uniaxial in-plane anisotropy field, respectively. It is to be noted that M_{eff} differs from M_S determined from magnetostatic SQUID measurements. The expression for M_{eff} is given in [44] as $4\pi M_{eff} = 4\pi M_S - H_\perp$, where $H_\perp$ is a sum of all possible perpendicular anisotropy fields—magnetoelastic, magnetocrystalline and Neel surface anisotropy. Apart perpendicular magnetic anisotropy, additional difference between M_S and M_{eff} can arise due to the fact that static SQUID measurements are magnetic-volume dependent, while FMR ones are independent. If sufficient volume of nonmagnetic material is present in the sample (like thick magnetically dead oxide layer on the surfase), experimentally determined $M_{eff} > M_S$.

Frequency dependence of PSSW was used to extract the exchange stiffness constant *A*. In [45] f_{PSSW} was given as:

$$f_{PSSW} = \frac{\gamma}{2\pi} \left[\begin{array}{c} \left(H_{ext} + H_{ani} + \frac{2A}{M_{eff}}\left(\frac{p\pi}{d}\right)^2\right) \times \\ \times \left(H_{ext} + H_{ani} + \frac{2A}{M_{eff}}\left(\frac{p\pi}{d}\right)^2 + 4\pi M_{eff}\right) \end{array} \right]^{1/2} \qquad (3)$$

where, *p* is the order of PSSW (*p* = 1 in our case) and *d* is the thickness of the film.

Dependence of the FMR frequency and the first order PSSW vs. H_{ext} are shown in Figure 5. Lines represent fit of the experimental data for f_{FMR} and f_{PSSW} using Equations (2) and (3), respectively. Estimated values of M_{eff} and *A* are presented in Table 2. The in-plane anisotropy H_{ani} extracted using Equation (2) was found to be vanishing (<10 Oe for all cases). It is in a good agreement with prediction that for fine polycrystalline films (like ours) H_{ani} can be neglected due to the randomization of the magnetocrystalline anisotropy axis within sample volume [17]. The gyromagnetic ratio $\gamma/2\pi$ shows no significant variation both with T_S and T_a. The estimated values are within 2.86–2.88 MHz/Oe. These correspond to the g-factor of 2.04–2.06 that point on weak spin-orbit interactions and correlates well with the earlier reports on Co_2FeGe films of different compositions [5].
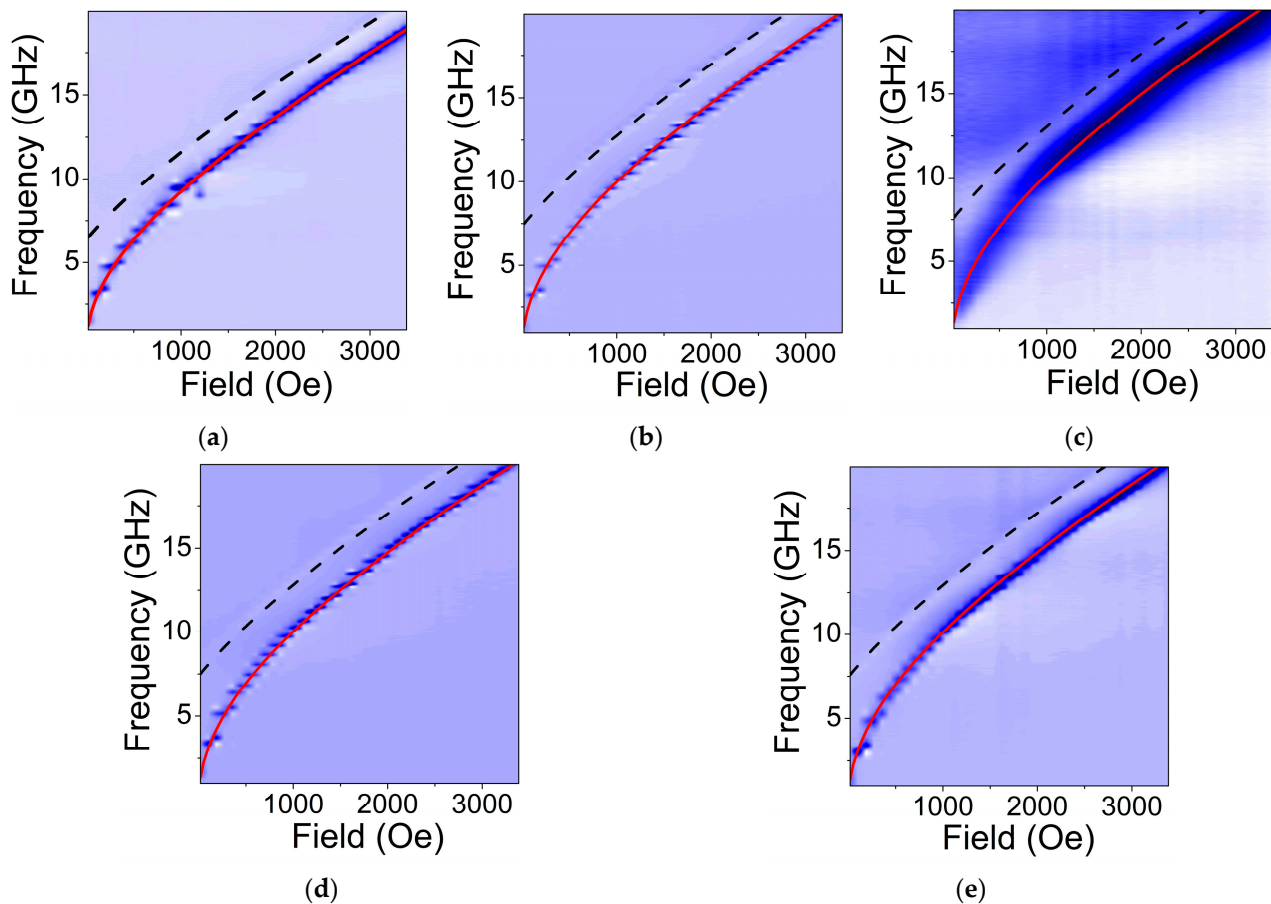
Figure 5. Dependencies of the FMR frequency and the first order PSSW on applied magnetic field for Co_2FeGe films deposited at various conditions: (**a**) T_S = RT; (**b**) T_S = 573 K; (**c**) T_S = 773 K; (**d**) T_S = RT+ annealing at T_a = 573 K for 1 h; (**e**) T_S = RT+ annealing at T_a = 773 K for 1 h. Solid red lines represent fit of the experimental data for FMR using Equation (2). Dashed lines represent fit for the first order PSSW using Equation (3). The values of effective magnetization M_{eff} and the exchange stiffness constant *A* extracted from the fitting are listed in Table 2.

Significant linewidth broadening was observed for the film deposited at T_S = 773 K. For this case the magnetic parameters were evaluated from FMR measurements with higher

uncertainty in comparison with the other films. For all films, apart the one deposited at $T_S = 773$ K, the values of M_{eff} determined by FMR correlates within experimental error with M_S from static SQUID measurements. This indicates that no significant out-of-plane anisotropies are presented in the films under study. Exchange stiffness constant for as-deposited films is relatively low $A \sim 6.8$ pJ/m. Both elevated T_S and annealing lead to the rise of A. However, the highest achieved values $A \sim 9 - 10$ pJ/m are still lower than for epitaxial $Co_{1.5}Fe_{1.5}Ge$ films ($A = 13$ pJ/m) [22]. It is well known [46] that the decrease of the exchange constant is associated with dilution magnetic atoms by non-magnetic. In our case for as deposited films Ge atoms are randomly placed within the crystal lattice leading to effective reduction of A. Elevated T_S and annealing lead to the improved atomic ordering and to the consequent increase of exchange stiffness, although it does not reach the values of epitaxial Co_2FeGe films with well-ordered structure. In addition, from EDAX data the films show an excess of Ge. This also can explain the reduction of A as the proportion of non-magnetic atoms is higher. One should keep in mind that the estimation of A in our case is relatively rough. First, the thickness of the films $d = 60$ nm was used for the estimation. The 'dead' magnetic layer associated with native surface oxide and crystallite boundaries in nanostructured films were not considered in the calculations because the estimation of their actual ratio is speculative. Second, only the 1st order standing spin wave was observed in the experiment leading to limitations in applicability of the Equation (3) [47].

Finally, Gilbert damping parameter α can be determined from FMR linewidth ΔH using the formula [28]:

$$\Delta H = \Delta H_0 + \frac{4\pi\alpha f}{\gamma} \tag{4}$$

where ΔH_0 is a measure of inhomogeneous broadening related to films quality. It is to be pointed out that linewidth broadening generally contains contributions from the intrinsic (Gilbert damping) and extrinsic (two-magnon scattering, inhomogeneity of magnetic properties in the measured material, angular dispersion of crystallite orientation) mechanisms.

Previously it was shown that for CoFeGe films with thickness above 50 nm [5] contribution from two magnon scattering [48] is negligible. It was mentioned in [49] that two-magnon scattering can add non-linear contribution to the $\Delta H(f)$ dependence that was not observed in our measurements. Indeed, our experimental data is fitted fairly well using linear dependence, Equation (4). Fitting results are presented in Figure 6 and estimated values of α listed in Table 2.
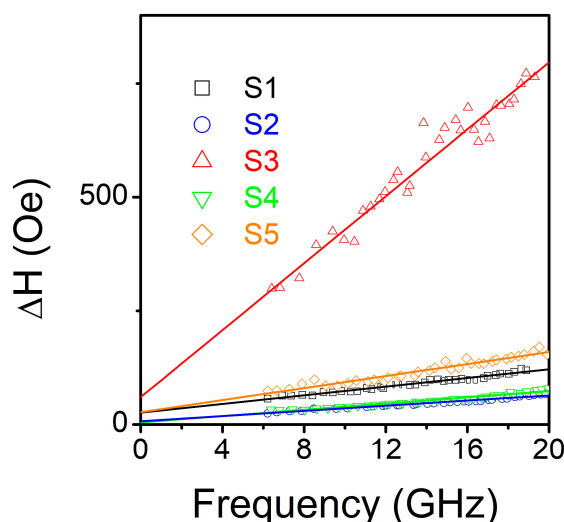
Figure 6. Dependencies of FMR linewidth ΔH as a function of resonance frequency for Co_2FeGe films deposited at $T_S = RT$ (S1), $T_S = 573$ K (S2), $T_S = 773$ K (S3) and deposited at RT and annealed for 1 h at $T_a = 573$ K (S4), $T_a = 773$ K (S5). Experimental data (points) are accompanied by fit (lines) according to Equation (3). Estimated values of damping parameter α are listed in Table 2.

Damping parameter α depends non-monotonically on both T_S and T_a. It is already relatively low for as deposited films (~0.007) and first decrease with T_S (or T_a). The minimal value of $\alpha \sim 0.004$ was observed for the film deposited at $T_S = 573$ K, and similar $\alpha \sim 0.005$ was obtained for $T_a = 573$ K. These values are consistent with reported earlier for CoFe-Ge films, although do not reach the lower limit [5,19,22] ~0.0025. This can be explained by the difference in microstructure of the films under investigation. Films in the abovementioned works were grown epitaxially on MgO single-crystalline substrates, while ours are polycrystalline. It is known [50] that grain boundaries cause non-uniformity in the internal magnetizing field or in demagnetizing field due to the internal defect. Another possible reason is that the chemical composition of our films (in particular, CoFe alloy component) is different from the one in the citing references. However, the values of α obtained in this work are smaller than those reported earlier for epitaxial $Co_2Fe(Ge_{0.5}Ga_{0.5})$ [51], widely used CoFeB [52] and some Co_2FeSi [18] films.

The further increase of processing temperature leads to the increase of α, slight in the case of annealing, or drastic ($\alpha \sim 0.06$) for $T_S = 773$ K. In these cases, the films are characterized by reduced lattice parameter with respect to bulk Co_2FeGe phase. In addition, this film shows higher surface roughness. A noticeable increase of damping was reported for Co_2FeSi films annealed at the elevated temperatures [53]. It was attributed to the influence of Cr buffer and atomic intermixture on Cr/Co_2FeSi interface. In our case no buffer or capping layers were used. Thus, additional contributions to damping associated with variation of chemical composition, tense stress, formation of textured structure and surface effects [18,54] should be considered.

From magnetic measurements one can evaluate the exchange length l_{ex}, an important parameter that dictates magnetization reversal [55]. It is essential for practical applications and micromagnetic simulations and can be described as the distance over which the perturbation due to the switching of a single spin decays in a soft magnetic material [56]. In [55] it was given as $l_{ex} = \sqrt{\frac{A}{2\pi M_S^2}}$. Using values from Table 2 one can get $l_{ex} \sim 4.6$ nm for the film deposited at $T_S = $ RT and $l_{ex} \sim 4.2$ nm for the film deposited at $T_S = 573$ K. The case of $T_S = 773$ K was not evaluated here because of big experimental error in determination of A associated with broadening of the FMR line. The annealing does not lead to significant changes in l_{ex}. The values of l_{ex} determined here are slightly lower comparing to those of CoFeB [52] and $Co_{1.5}Fe_{1.5}Ge$ [22] films and are typical for soft magnetic materials [55].

It is interesting to note that according to the data reported in [19], annealing at $T_a = 673$ K leads to the increase of damping for $Fe_{1.5}CoGe$ films, while for $T_a = 773$ K no visible FMR peak was found, suggesting the degradation of magnetic properties with increased T_a. Contrary to this, broadened FMR resonance peaks are still visible for our films deposited or annealed at 773 K. Simultaneously, slight decrease in M_S and strong increase of H_C and α were observed at $T_S = 773$ K. Thus, one can conclude that the growth conditions associated with $T_S = 773$ K cause a degrading effect on dynamic magnetic properties of the Co_2FeGe films. A suggestion can be made that the effect of a compressive stress or formation of the film with strong contribution from crystalline anisotropy is a cause for such behavior. Physical mechanisms associated with these variations should be studied carefully in the future works.

4. Conclusions

Polycrystalline Co_2FeGe Heusler alloy films with close to stoichiometry composition were fabricated using DC-magnetron co-sputtering technique from Co_2Fe and Ge targets. Influence of deposition conditions, namely, substrate temperature and post-deposition annealing on magnetic properties was studied. Elevated substrate temperature and annealing promote formation of ordered $L2_1$ phase. Damping parameter α as low as 0.004 was achieved. This value is consistent with predicted for half-metallic compounds having a gap in minority density of states on Fermi level. It was found that saturation magnetization and exchange stiffness constant for the investigated films are relatively low. Our study demon-

strates that the crystal structure, grain size and roughness can be controlled by adequate growth conditions and consequently, both static and dynamic magnetic properties could be effectively tuned in a wide range using these parameters. This paves the way to a possible future technological application of these films as some of them present the proper magnetic properties (low damping parameter, saturation magnetization and exchange stiffness) for spin-transfer torque devices with reduced operation current.

Author Contributions: Conceptualization, A.V. and J.P.A.; methodology, A.V.; validation, A.V. and J.P.A.; formal analysis, A.V., S.A.B. and G.N.K.; investigation, A.V., S.A.B., P.Š., N.R.V., B.P., A.A., J.Á.P. and G.N.K.; resources, J.Á.P., P.A.A., G.N.K. and J.P.A.; data curation, A.V., S.A.B., P.Š., B.P., J.Á.P., P.A.A. and G.N.K.; writing—original draft preparation, A.V and G.N.K.; writing—review and editing, A.V., J.Á.P., P.A.A., G.N.K. and J.P.A.; supervision, J.P.A.; project administration, G.N.K. and J.P.A.; funding acquisition, P.A.A. and J.P.A. All authors have read and agreed to the published version of the manuscript.

Data Availability Statement: The data presented in this study are available on request from the corresponding author.

Conflicts of Interest: The authors declare that they have no known competing financial interests or personal relationships that could have appeared to influence the work reported in this paper.

References

1. Felser, C.; Hirohata, A. (Eds.) *Heusler Alloys Properties, Growth, Applications*; Springer International Publishing: Basel, Switzerland, 2016; pp. 1–486.
2. Balke, B.; Wurmehl, S.; Fecher, G.H.; Felser, C.; Kübler, J. Rational design of new materials for spintronics: Co_2FeZ (Z = Al, Ga, Si, Ge). *Sci. Technol. Adv. Mater.* **2008**, *9*, 014102. [CrossRef]
3. Locatelli, N.; Cros, V.; Grollier, J. Spin-torque building blocks. *Nat. Mater.* **2014**, *13*, 11–20. [CrossRef] [PubMed]
4. Trudel, S.; Gaier, O.; Hamrle, J.; Hillebrands, B. Magnetic anisotropy, exchange and damping in cobalt-based full-Heusler compounds: An experimental review. *J. Phys. D Appl. Phys.* **2010**, *43*, 193001. [CrossRef]
5. Lee, H.; Wang, Y.-H.A.; Mewes, C.K.A.; Butler, W.H.; Mewes, T.; Maat, S.; York, B.; Carey, M.J.; Childress, J.R. Magnetization relaxation and structure of CoFeGe alloys. *Appl. Phys. Lett.* **2009**, *95*, 082502. [CrossRef]
6. Uvarov, N.V.; Kudryavtsev, Y.V.; Kravets, A.F.; Vovk, A.Y.; Borges, R.P.; Godinho, M.; Korenivski, V. Electronic structure, optical and magnetic properties of Co_2FeGe Heusler alloy films. *J. Appl. Phys.* **2012**, *112*, 063909. [CrossRef]
7. Gercsi, Z.; Hono, K. *Ab initio* predictions for the effect of disorder and quarternary alloying on the half-metallic properties of selected Co_2Fe-based Heusler alloys. *J. Phys. Condens. Matter* **2007**, *19*, 326216. [CrossRef]
8. Wurmehl, S.; Fecher, G.H.; Kandpal, H.C.; Ksenofontov, V.; Felser, C.; Lin, H.-J.; Morais, J. Geometric, electronic, and magnetic structure of Co_2FeSi: Curie temperature and magnetic moment measurements and calculations. *Phys. Rev. B* **2005**, *72*, 184434. [CrossRef]
9. Kruglyak, V.V.; Demokritov, S.O.; Grundler, D. Magnonics. *J. Phys. D Appl. Phys.* **2010**, *43*, 264001. [CrossRef]
10. Gilbert, T.L. A phenomenological theory of damping in ferromagnetic materials. *IEEE Trans. Magn.* **2004**, *40*, 3443–3449. [CrossRef]
11. Mizukami, S.; Watanabe, D.; Oogane, M.; Ando, Y.; Miura, Y.; Shirai, M.; Miyazaki, T. Low damping constant for Co_2FeAl Heusler alloy films and its correlation with density of states. *J. Appl. Phys.* **2009**, *105*, 07D306. [CrossRef]
12. Yilgin, R.; Sakuraba, Y.; Oogane, M.; Mizukami, S.; Ando, Y.; Miyazaki, T. Anisotropic intrinsic damping constant of epitaxial Co_2MnSi Heusler alloy films. *Jpn. J. Appl. Phys.* **2007**, *46*, L205–L208. [CrossRef]
13. Guillemard, C.; Petit-Watelot, S.; Pasquier, L.; Pierre, D.; Ghanbaja, J.; Rojas-Sánchez, J.-C.; Bataille, A.; Rault, J.; Le Fèvre, P.; Bertran, F.; et al. Ultralow magnetic damping in Co_2Mn-based Heusler compounds: Promising materials for spintronics. *Phys. Rev. Appl.* **2019**, *11*, 064009. [CrossRef]
14. Kambersky, V. On the Landau–Lifshitz relaxation in ferromagnetic metals. *Can. J. Phys.* **1970**, *48*, 2906–2911. [CrossRef]
15. Galanakis, I. Orbital magnetism in the half-metallic Heusler alloys. *Phys. Rev. B* **2005**, *71*, 012413. [CrossRef]
16. Slonczewski, J.C. Excitation of spin waves by an electric current. *J. Magn. Magn. Mater.* **1999**, *195*, L261–L268. [CrossRef]
17. Hazra, B.K.; Kaul, S.N.; Srinath, S.; Raja, M.M. Uniaxial anisotropy, intrinsic and extrinsic damping in Co_2FeSi Heusler alloy thin films. *J. Phys. D Appl. Phys.* **2019**, *52*, 325002. [CrossRef]

18. Koehler, A.; Wollmann, L.; Ebke, D.; Chadov, S.; Kaiser, C.; Diao, Z.; Zheng, Y.; Leng, Q.; Felser, C. Tunable damping in the Heusler compound $Co_{2-x}Ir_xMnSi$. *Phys. Rev. B* **2016**, *93*, 094410. [CrossRef]
19. Conca, A.; Niesen, A.; Reiss, G.; Hillebrands, B. Low damping magnetic properties and perpendicular magnetic anisotropy in the Heusler alloy $Fe_{1.5}CoGe$. *AIP Adv.* **2019**, *9*, 085205. [CrossRef]
20. Ryabchenko, S.M.; Kalita, V.M.; Kulik, M.M.; Lozenko, A.F.; Nevdacha, V.V.; Pogorily, A.N.; Kravets, A.F.; Podyalovskiy, D.Y.; Vovk, A.Y.; Borges, R.P.; et al. Rotatable magnetic anisotropy in $Si/SiO_2/(Co_2Fe)_xGe_{1-x}$ Heusler alloy films. *J. Phys. Condens. Matter* **2013**, *25*, 416003. [CrossRef] [PubMed]
21. Pogorily, A.N.; Kravets, A.F.; Nevdacha, V.V.; Podyalovskiy, D.Y.; Ryabchenko, S.M.; Kalita, V.M.; Kulik, M.M.; Lozenko, A.F.; Vovk, A.Y.; Godinho, M.; et al. Magnetic anisotropy of epitaxial Co_2Fe-Ge Heusler alloy films on MgO (100) substrates. *AIP Adv.* **2017**, *7*, 055831. [CrossRef]
22. Neggache, A.; Hauet, T.; Bertran, F.; Le Fevre, P.; Petit-Watelot, S.; Devolder, T.; Ohresser, P.; Boulet, P.; Mewes, C.; Maat, S.; et al. Testing epitaxial $Co_{1.5}Fe_{1.5}Ge(001)$ electrodes in MgO-based magnetic tunnel junctions. *Appl. Phys. Lett.* **2014**, *104*, 252412. [CrossRef]
23. Nakatani, N.; Imai, S.; Tanaka, M.A.; Kubota, T.; Takanashi, K.; Mibu, K. Deposition temperature dependence of interface magnetism of Co_2FeGe-Heusler-alloy/Ag films studied with ^{57}Fe Mössbauer spectroscopy. *J. Magn. Magn. Mater.* **2018**, *464*, 71–75. [CrossRef]
24. Kakazei, G.N.; Kravetz, A.F.; Lesnik, N.A.; Pereira de Azevedo, M.M.; Bondarkova, Y.G.; Silantiev, V.I.; Sousa, J.B. Influence of co-evaporation technique on the structural and magnetic properties of CoCu granular films. *J. Magn. Magn. Mater.* **1999**, *196–197*, 29–30. [CrossRef]
25. García-García, A.; Pardo, J.A.; Navarro, E.; Štrichovanec, P.; Vovk, A.; Morellón, L.; Algarabel, P.A.; Ibarra, M.R. Combinatorial pulsed laser deposition of Fe/MgO granular multilayers. *Appl. Phys. A* **2012**, *107*, 871–876. [CrossRef]
26. Garcia, M.A.; Fernandez Pinel, E.; de la Venta, J.; Quesada, A.; Bouzas, V.; Fernández, J.F.; Romero, J.J.; Martín González, M.S.; Costa-Krämer, J.L. Sources of experimental errors in the observation of nanoscale magnetism. *J. Appl. Phys.* **2009**, *105*, 013925. [CrossRef]
27. Pereira, L.M.C.; Araujo, J.P.; VanBael, M.J.; Temst, K.; Vantomme, A. Practical limits for detection of ferromagnetism using highly sensitive magnetometry techniques. *J. Phys D Appl. Phys.* **2011**, *44*, 215001. [CrossRef]
28. Kalarickal, S.S.; Krivosik, P.; Wu, M.; Patton, C.E.; Schneider, M.L.; Kabos, P.; Silva, T.J.; Nibarger, J.P. Ferromagnetic resonance linewidth in metallic thin films: Comparison of measurement methods. *J. Appl. Phys.* **2006**, *99*, 093909. [CrossRef]
29. Tokaç, M.; Bunyaev, S.A.; Kakazei, G.N.; Schmool, D.S.; Atkinson, D.; Hindmarch, A.T. Interfacial structure dependent spin mixing conductance in cobalt thin films. *Phys. Rev. Lett.* **2015**, *115*, 056601. [CrossRef]
30. Sakuraba, Y.; Nakata, J.; Oogane, M.; Ando, Y.; Kato, H.; Sakuma, A.; Miyazaki, T.; Kubota, H. Magnetic tunnel junctions using *B*2-ordered Co_2MnAl Heusler alloy epitaxial electrode. *Appl. Phys. Lett.* **2006**, *88*, 022503. [CrossRef]
31. Heusler, O. Kristallstruktur und ferromagnetismus der Mangan-Aluminium-Kupferlegierungen. *Ann. Phys.* **1934**, *411*, 155–201. [CrossRef]
32. Balke, B.; Wurmehl, S.; Fecher, G.H.; Felser, C.; Alves, M.C.M.; Bernardi, F.; Morais, J. Structural characterization of the Co_2FeZ (*Z*=Al, Si, Ga, and Ge) Heusler compounds by x-ray diffraction and extended x-ray absorption fine structure spectroscopy. *Appl. Phys. Lett.* **2007**, *90*, 172501. [CrossRef]
33. Inorganic Crystal Structure Database, 01-082-8750. Available online: https://icsd.products.fiz-karlsruhe.de/en (accessed on 1 September 2015).
34. Wurmehl, S.; Wójcik, M. Structural Order in Heusler Compounds. In *Heusler Alloys Properties, Growth, Applications*; Felser, C., Hirohata, A., Eds.; Springer International Publishing: Basel, Switzerland, 2016; pp. 87–110.
35. Graf, T.; Casper, F.; Winterlik, J.; Balke, B.; Fecher, G.H.; Felser, C. Crystal structure of new Heusler compounds. *Z. Anorg. Allg. Chem.* **2009**, *635*, 976–981. [CrossRef]
36. Patterson, A.L. The Scherrer formula for X-Ray particle size determination. *Phys. Rev.* **1939**, *56*, 978–982. [CrossRef]
37. Buschow, K.H.J.; van Engen, P.G.; Jongebreur, R. Magneto-optical properties of metallic ferromagnetic materials. *J. Magn. Magn. Matter.* **1983**, *38*, 1–22. [CrossRef]
38. Kandpal, H.C.; Fecher, G.H.; Felser, C. Calculated electronic and magnetic properties of the half-metallic, transition metal based Heusler compounds. *J. Phys. D Appl. Phys.* **2007**, *40*, 1507–1523. [CrossRef]
39. Maat, S.; Carey, M.J.; Childress, J.R. Current perpendicular to the plane spin-valves with CoFeGe magnetic layers. *Appl. Phys. Lett.* **2008**, *93*, 143505. [CrossRef]
40. Kumar, K.R.; Bharathi, K.K.; Chelvane, J.A.; Venkatesh, S.; Markandeyulu, G.; Harishkumar, N. First-Principles Calculation and Experimental Investigations on Full-Heusler Alloy Co_2FeGe. *IEEE Trans. Magn.* **2009**, *45*, 3997–3999. [CrossRef]
41. Takamura, Y.; Nishijima, A.; Nagahama, Y.; Nakane, R.; Sugahara, S. Formation of Si- and Ge-based Full-Heusler Alloy thin tilms using SOI and GOI substrates for the Half-metallic source and drain of spin transistors. *ECS Trans.* **2008**, *16*, 945–952. [CrossRef]
42. Sterwerf, C.; Paul, S.; Khodadadi, B.; Meinert, M.; Schmalhorst, J.-M.; Buchmeier, M.; Mewes, C.K.A.; Mewes, T.; Reiss, G. Low Gilbert damping in Co_2FeSi and Fe_2CoSi films. *J. Appl. Phys.* **2016**, *120*, 083904. [CrossRef]
43. Kittel, C. On the theory of ferromagnetic resonance absorption. *Phys. Rev.* **1948**, *73*, 155–161. [CrossRef]

44. Kakazei, G.N.; Wigen, P.E.; Guslienko, K.Y.; Chantrell, R.W.; Lesnik, N.A.; Metlushko, V.; Shima, H.; Fukamichi, K.; Otani, Y.; Novosad, V. In-plane and out-of-plane uniaxial anisotropies in rectangular arrays of circular dots studied by ferromagnetic resonance. *J. Appl. Phys.* **2003**, *93*, 8418–8420. [CrossRef]

45. Demokritov, S.O.; Hillebrands, B. Spinwaves in Laterally Confined Magnetic Structures. In *Spin Dynamics in Confined Magnetic Structures I*; Hillebrands, B., Ounatjela, K., Eds.; Springer International Publishing: Basel, Switzerland, 2002; pp. 65–93.

46. Kittel, C. *Introduction to Solid State Physics*, 7th ed.; John Wiley & Sons: New York, NY, USA, 1996; pp. 1–675.

47. Dobrovolskiy, O.V.; Bunyaev, S.A.; Vovk, N.R.; Navas, D.; Gruszecki, P.; Krawczyk, M.; Sachser, R.; Huth, M.; Chumak, A.V.; Guslienko, K.Y.; et al. Spin-wave spectroscopy of individual ferromagnetic nanodisks. *Nanoscale* **2020**, *12*, 21207. [CrossRef]

48. McMichael, R.D.; Krivosik, P. Classical model of extrinsic ferromagnetic resonance linewidth in ultrathin films. *IEEE Trans. Magn.* **2004**, *40*, 2–10. [CrossRef]

49. Arias, R.; Mills, D.L. Extrinsic contributions to the ferromagnetic resonance response of ultrathin films. *Phys. Rev. B* **1999**, *60*, 7395–7409. [CrossRef]

50. Yilgin, R.; Oogane, M.; Ando, Y.; Miyazaki, T. Gilbert damping constant in polycrystalline Co_2MnSi Heusler alloy films. *J. Magn. Magn. Mater.* **2007**, *310*, 2322–2323. [CrossRef]

51. Varaprasad, B.S.D.C.S.; Srinivasan, A.; Takahashi, Y.K.; Hayashi, M.; Rajanikanth, A.; Hono, K. Spin polarization and Gilbert damping of $Co_2Fe(Ga_xGe_{1-x})$ Heusler alloys. *Acta Mater.* **2012**, *60*, 6257–6265. [CrossRef]

52. Conca, A.; Papaioannou, E.T.; Klingler, S.; Greser, J.; Sebastian, T.; Leven, B.; Lösch, J.; Hillebrands, B. Annealing influence on the Gilbert damping parameter and the exchange constant of CoFeB thin films. *Appl. Phys. Lett.* **2014**, *104*, 182407. [CrossRef]

53. Oogane, M.; Yilgin, R.; Shinano, M.; Yakata, S.; Sakuraba, Y.; Ando, Y.; Miyazaki, T. Magnetic damping constant of Co_2FeSi Heusler alloy thin film. *J. Appl. Phys.* **2007**, *101*, 09J501. [CrossRef]

54. Kasatani, Y.; Yamada, S.; Itoh, H.; Miyao, M.; Hamaya, K.; Nozaki, Y. Large anisotropy of Gilbert damping constant in $L2_1$-ordered Co_2FeSi film. *Appl. Phys. Express* **2014**, *7*, 123001. [CrossRef]

55. Abo, G.S.; Hong, Y.-K.; Park, J.; Lee, J.; Lee, W.; Choi, B.-C. Definition of magnetic exchange length. *IEEE Trans. Magn.* **2013**, *49*, 4937–4939. [CrossRef]

56. McHenry, M.E.; Laughlin, D.E. Nano-scale materials development for future magnetic applications. *Acta Mater.* **2000**, *48*, 223–238. [CrossRef]